Polymer Engineering & Science

WILEY | spe INSPIRING PLASTICS PROFESSIONALS

RESEARCH ARTICLE OPEN ACCESS

Data-Driven Design of Co-Continuous Morphology in PS/PMMA Two-Phase Polymer Blends: A Theoretical, Experimental, and Machine Learning Approach

Juan Felipe Castro-Landinez[1] | Tasmai Paul[2] | Rodrigo Q. Albuquerque[1,3] | Holger Schmalz[2,4] | Andreas Greiner[2,4] | Holger Ruckdäschel[1,3]

[1]Polymer Engineering, University of Bayreuth, Bayreuth, Germany | [2]Macromolecular Chemistry, University of Bayreuth, Bayreuth, Germany | [3]Neue Materialien Bayreuth GmbH, Bayreuth, Germany | [4]Bavarian Polymer Institute, University of Bayreuth, Bayreuth, Germany

Correspondence: Holger Ruckdäschel (holger.ruckdaeschel@uni-bayreuth.de)

Received: 24 November 2025 | **Revised:** 16 February 2026 | **Accepted:** 17 March 2026

Keywords: Bayesian optimization - Machine learning | copolymer compatibilization | immiscible polymer blends | melt blending | morphology analysis | rheological performance

ABSTRACT

The morphological control of immiscible polymer blends is critical for tailoring material properties, yet predicting phase structures remains challenging. This study combines theoretical modeling, experimental characterization, and machine learning to analyze morphologies in polystyrene/poly(methyl methacrylate) (PS/PMMA) blends. Phase inversion compositions were predicted using Utracki and Yu-Bousmina-Schreiber models at 60–68 wt% PMMA, correlating well with transmission electron microscopy observations. A PS-*b*-PMMA diblock copolymer compatibilizer effectively stabilized morphologies and broadened the co-continuous region. A co-continuity index (CCI*) quantified morphological characteristics, revealing maximum co-continuity (CCI* = 0.70–0.86) in the 40–60 wt% PMMA range. Bayesian optimization identified optimal processing windows with minimal experiments, while machine learning models, particularly random forest, successfully predicted co-continuity indices. Compositional factors dominated morphology formation over processing conditions. This integrated methodology provides an efficient framework for accelerating polymer blend development with reduced experiments required.

1 | Introduction

Properties and processing methods for several polymeric blend materials have been extensively researched over the last decades [1–3]. The main purpose of polymer blending is either to obtain certain tailored properties, expanding the application range of materials, or getting a requested property for a specific application [4]. Research on polymer blends started with the understanding of miscibility definition [5, 6], later in compatibilizers (such as graft and block copolymer) addition [7], then in morphology formation and mixing techniques [8, 9], and recently in optimization methods to selectively get morphologies to obtain desired properties [2, 10].

For immiscible polymers, phase domain refinement has proven to be a powerful solution to enhance their properties [11]. These blends have been investigated extensively for coatings, lithography, water treatment, catalysis, solar cells, among other applications [12–14]. One example of immiscible blends is PMMA and PS. In this case, it is shown that phase morphology is driven by the ratio of polymers, in which the major component will be the matrix and the other will form

Highlights

- Machine learning design of polymer blends with tailored interconnected networks
- Tool to assess co-continuity from TEM images and guide blend design
- Theory and experiments to study phase inversion in polymer blends.
- Study of a diblock copolymer's role as compatibilizer in blend morphology.

the dispersed phase [15]. However, for similar proportions of components, the morphology formation will be driven by the viscosity ratio at the processing conditions [8].

In thermodynamically immiscible PS/PMMA blends, coalescence during processing is usually avoided by using compatibilization strategies. A common approach is to use graft copolymers or block copolymers (BCP) as compatibilizers. For the latter, a low molecular weight of the BCP must be ensured so it will tend to stay at the interface of the phases rather than creating micelles or separated phases [16]. Although BCPs represent challenges during processing and blending, they can be used in reduced amounts [7]. By this compatibilization, the interfacial tension between PS and PMMA is reduced, resulting in a phase size reduction of the dispersed phase as shown, for example, by Thomas and Prud'homme [17] using PS-*b*-PMMA diblock copolymers.

By achieving a finer morphology of the dispersed phases, several authors have demonstrated improvement in different properties for the examined blends. For instance, Yee et al. [18] observed that by adding a random PS-*ran*-PMMA copolymer the interfacial tension is reduced and the resistance of the interfacial layer to shear is increased, reducing the size of the dispersed phase. Bussi et al. [19] were able to produce a compatibilized PS/PMMA membrane that is effective for high water flux, keeping a good chemical and mechanical performance by tuning morphology. In another blend case, Bubmann et al. [20] reported getting a transparent PC/PMMA blend via reactive extrusion (in situ formation of a PC/PMMA copolymer during compounding), having finer co-continuous morphologies and improved optical properties.

Furthermore, Wu et al. [11, 21] tried a different approach, not using compatibilizers for reducing the size of the dispersed phase but processing with a different methodology (water-assisted extrusion mixing). Their blends, showing reduced phase size, had an improvement in creep, elongation at break, and tensile strength resistance. Commonly, in the case of melt blending, residence time, temperature, and rotational speed indicate the rheological state of a material which may affect the final morphology and properties [16]. Theoretically, catching the effect of compatibilization on the phase morphology remains challenging; several indirect testing methods should be included to demonstrate such compatibilization or modifications on morphologies. Therefore, investigating both compatibilizing techniques as well as the rheological behavior at processing conditions to understand morphology formation is paramount.

Although most of the methodologies for evaluating polymeric blends are well described, these usually require larger amounts of material and time for experimental runs. Choosing a well-known system, such as PS/PMMA, to tailor its morphology by varying the processing states was beneficial for the research presented in this article. Therefore, the aim of this research was to establish a methodology capable of identifying the operational processing and compositional window, in which a particular co-continuous morphology is obtained; aiming for the highest interconnected network possible by training a machine learning (ML) model based on Bayesian optimization (BO).

The study shows the relationship between the morphology and properties of the blends with different levels evaluated experimentally. Including, especially, the direct effect of the processing parameter and compatibilizer content on immiscible blend morphologies. The results provide a relevant understanding on how to approach melt blending testing theoretically and experimentally, by obtaining critical information for training a Bayesian optimization model. This reduces the number of experiments, the amount of material, and the time required during the investigation of polymer blends and composites.

2 | Materials and Methods

2.1 | Materials

Three different grades of polystyrene (PS) with distinct molecular weight (Low molecular weight Styrolution 153N: PS-LM_W; middle molecular weight Styrolution 158N: PS-MM_W; high molecular weight Styrolution 168N: PS-HM_W) were kindly provided by Ineos Styrolution Europe GmbH. Poly(methyl methacrylate) (PMMA, Plexiglas 8N) was provided by Röhm GmbH. Relevant properties of the neat materials are listed in Table 1. For the synthesis of the PS-*b*-PMMA diblock copolymer, styrene (Sigma

TABLE 1 | Selected properties of the materials used in blend screening and testing.

		Properties		
Material	**References**	**Density ($g\,cm^{-3}$)**	**MFI[a] ($cm^3\,10\,min^{-1}$)**	**M_w ($kg\,mol^{-1}$)**
PS-LM_W	153N	1.04	17.00	197
PS-MM_W	158N	1.04	3.30	212
PS-HM_W	168N	1.04	1.50	273
PMMA	8N	3.00	1.19	124

[a]MFI: PS (200°C, 5 kg) and PMMA (230°C, 3.8 kg).

Aldrich, 4-*tert*-butylcatechole stabilized, ≥ 99%), methyl methacrylate (MMA, Sigma Aldrich, ≥ 99%), 1,1-diphenylethylene (DPE, TCI, ≥98%), *sec*-butyllithium (*sec*-BuLi, Thermo Scientific, 1.3 M in cyclohexane), dibutyl magnesium (DBM, Sigma Aldrich 1 M in heptane), triethylaluminium (TEAl, Sigma Aldrich, 1 M in hexane), methanol (Fluka, p.a., ≥ 99.9%) and technical grade ethanol were used. Tetrahydrofuran (THF, Thermo Fisher Scientific, 99.9%, extra pure) for anionic polymerization was successively distilled over calcium hydride and elemental potassium under dry nitrogen atmosphere for 2–3 days each. DPE was purified over *sec*-BuLi under dry argon followed by vacuum distillation. The purified DPE was stored in a Schlenk tube under dry nitrogen in a fridge until use. Styrene was degassed by three consecutive freeze–thaw cycles on a high vacuum line, stirred over DBM for 1–2 h, condensed in a glass ampoule and stored over night frozen in liquid nitrogen. A similar procedure was employed for MMA except using TEAl for purification and the purified MMA was directly used for polymerization.

2.2 | Diblock Copolymer Synthesis

Anionic polymerization was conducted in a (3 L) double jacketed laboratory glass reactor (Büchi AG) filled with (2.2 ~ L) THF and equipped with an ultra-cryostat. The presence of lithium alkoxides is necessary for a controlled living polymerization of MMA resulting in low dispersities. Accordingly, lithium alkoxides were produced in situ prior to polymerization by the addition of *sec*-BuLi to THF (ca. 1 mL per 100 mL THF) at −60°C followed by heating to 25°C. This induces deprotonation and subsequent decomposition of THF to ethylene and the respective lithium ethenolate. Polymerization of styrene was initiated with *sec*-BuLi and allowed to proceed for 15 min at −70°C. Subsequently, DPE (5 eq. with respect to *sec*-BuLi) was added to the living polystyryllithium to reduce the nucleophilicity of the active chain end for the subsequent MMA polymerization. After stirring for 30 min the desired amount of MMA was added and polymerization was stopped after another 30 min by the addition of degassed methanol. The PS-*b*-PMMA diblock copolymer was isolated by precipitation from ethanol and dried under vacuum (yield: 127 g, M_n: 90000 g mol^{-1}, $Đ$: 1.08, 47 wt.% PS). The molecular weight distribution and morphology of the BCP are shown in the Figures S5 and S6.

2.3 | Melt Blending and Characterization Methods

Prior to melt blending, all materials were dried under vacuum at 80°C overnight. Neat materials and blends were processed in a twin screw micro-compounder MC 15 HT Xplore, varying processing conditions such as temperature, residence time, and rotational speed. The parameters of the experimental design are summarized in Table 2 and the employed blend compositions are given in the Table S1. In this paper, different blend proportions with several additions of BCP are used. The blend compositions were designed gravimetrically, and for ease of annotation, were labeled as, for example, PS/PMMA/BCP 50/50/2; which contains 2 wt% of BCP and the rest will be equal proportion of PS/PMMA blend. The extruded materials were converted into granulates of 3 mm, then hot pressed in a PW-20H-HKP500 laboratory press at 220°C with a preheating time of 5 min, a first force applied of 25 kN for 1 min to mitigate bubbles, an applied secondary force of 90 kN for 2 min, and finally placed in a secondary press with water cooling system at room temperature.

TABLE 2 | Parameters for melt compounding.

Factor	Units	Min-value	Max-value	Step
PMMA-content	(wt%)	0	100	0.1
PS-content	(wt%)	0	100	0.1
BCP-content (PS-*b*-PMMA)	(wt%)	0	8	0.1
Temperature	(°C)	200	250	1
Rotational speed	(rpm)	60	150	1
Residence time	(min)	3	10	0.5

Rheological characterization was performed with a Rheometrics Dynamic Analyzer RDA III using a parallel plate configuration with a plate diameter of 25 mm and a gap of 1 mm. Prior to each measurement, a strain sweep was run to determine the linear viscoelastic region. Frequency sweeps were conducted from 0.01 to 500 rad s^{-1} at temperatures between 160°C and 240°C.

Thermo-mechanical properties were determined using a DMA Gabo Eplexor 500N in tension under nitrogen with samples of $50 \times 10 \times 1$ mm^3. A static and dynamic load of 0.5% and 0.1% was defined, and a temperature ramp (3°C min^{-1}) starting from 30°C to 140°C was done to catch the glass transition temperature of the materials. Storage modulus, loss modulus, and loss factor were extracted from the measurement. Differential Scanning Calorimetry (DSC) was also performed to confirm phases and possible modifications on transition temperatures of the blends. The DSC Mettler Toledo 1 was set up in a heating–cooling–heating method between 25°C and 250°C with a ramp of 10°C min^{-1} and under a nitrogen atmosphere.

Finally, the morphology of the polymer blends was characterized via transmission electron microscopy (JEOL JEM-2200FS) at an acceleration voltage of 200 kV. The samples were cut using an ultramicrotome (Leica EM UC7) and then treated with RuO_4 vapor to selectively stain the PS phases in the blends.

2.4 | Machine Learning Methods

The Bayesian optimization (BO) methodology is capable of maximizing and/or minimizing one or more target properties based on the different independent variables (features or factors) that affect it, as it is already shown in previous studies [22–24]. In particular, in the case of polymer blends, the features are related to the composition and processing parameters [15, 17, 25]. Gaussian processes (GP) are usually applied as regressor models, as they have the ability to provide both a predicted mean

value and the corresponding uncertainty (standard deviation). The maximum expected improvement was used as the acquisition function. The radial basis function (RBF) or Matern kernels were used to build the covariance matrix of the GP model in each iteration.

In this research, an initial set of experiments was defined taking into account the parameters mentioned in Table 2 as well as the expected morphologies known in the literature. The defined output parameter in this case was the morphology obtained, with a higher co-continuous blend being targeted. A co-continuous index (CCI*) was defined in Equation (3) to evaluate the morphologies observed via TEM.

$$F_f = \frac{4\pi A}{P^2} \tag{1}$$

$$\mathrm{CI}_i = 1 - \frac{\sum A_i F_{f,i}}{\sum A_i} \tag{2}$$

$$\mathrm{CCI}^* = CI_{\mathrm{PMMA}} \times CI_{\mathrm{PS}} \tag{3}$$

where a shape factor F_f is calculated from the area A and the perimeter P of each individual phase evaluated, taken from the ASTM F1877-16 Standard Practice for Characterization of Particles, while the CI_i (Equation 2) corresponds to a continuity index defined for each individual polymer in the blend. These continuity degree explains how continuous each polymer phase is through the final blend morphology and it is calculated individually for each component, in this case PS and PMMA. These values were extracted from the TEM images obtained by an image analysis performed in Python. Using both $\mathrm{CI}_{\mathrm{PMMA}}$ and $\mathrm{CI}_{\mathrm{PS}}$ the CCI^* of the blend was calculated. As could be noticed in the definition, a value close to 1 implies a more co-continuous morphology while a value close to 0 is a highly dispersed type of morphology.

In general terms, the BO starts with an initial set of experimental data taken from the experimental set, a GP model is trained with the data, and then a new point (or experiment) is suggested by an acquisition function (maximum expected improvement in this case), which considers a tradeoff between exploitation (samples with high predictions are suggested) and exploration (samples with high predictive uncertainties are suggested) [22]. The BO algorithm searches for the best possible experiments in a big virtual dataset comprising millions of possible combinations of the factors. The newly selected combination of factors, corresponding to the next suggested experiment, is evaluated in the laboratory. The resulting measured target property is added to the dataset, which is then used to retrain the GP model for improved accuracy. This optimization loop is repeated iteratively, allowing the process to evolve toward maximizing the target property, eventually reaching a value close to 1.

For the BO rounds, we employed the Expected improvement (EI) acquisition function (Equation 4) with a weighting parameter of $\xi = 0.02$, which balances exploration and exploitation by favoring both promising regions of the design space and areas of higher uncertainty. For the Active Learning rounds, an uncertainty-based acquisition function was adopted, whereby candidate samples were selected solely based on their predictive uncertainty, independently of the corresponding target predictions. This strategy therefore emphasizes exploration of poorly sampled regions of the input space. In contrast, the Greedy strategy relies directly on the model predictions as the acquisition function, without accounting for predictive uncertainty, and thus prioritizes samples with the highest predicted target values.

$$\mathrm{EI}(\mathbf{x}) = \begin{cases} \left(\mu(\mathbf{x}) - f\left(\mathbf{x}^+\right) - \xi\right) \cdot \Phi(Z) + \sigma(\mathbf{x}) \cdot \phi(Z) \\ \qquad \text{if } \sigma(\mathbf{x}) > 0 \\ 0, \quad \text{otherwise} \end{cases} \tag{4}$$

where

$$Z = \frac{\mu(\mathbf{x}) - f\left(\mathbf{x}^+\right) - \xi}{\sigma(\mathbf{x})} \tag{5}$$

here $\mu(\mathbf{x})$ is the predicted mean and $\sigma(\mathbf{x})$ the predicted standard deviation at input $\mathbf{x}$. $f\left(\mathbf{x}^+\right)$ is the best observed function value so far, and ξ is a parameter controlling the trade-off between exploration and exploitation (set to 0.02 in this work). $\Phi(Z)$ and $\phi(Z)$ denote the cumulative distribution and probability density functions of the standard normal distribution, respectively.

In addition, a diverse set of machine learning (ML) regression models was applied to the final experimental dataset to explore how the input factors influence the target output. These models—readily available through Python libraries within the Jupyter Notebook environment—include random forest (RF), gradient boosting (GB), support vector regressor (SVR), Gaussian processes (GP), among others. Each model was screened to identify the best fit for the experimental data, based on formulations and algorithms detailed in references [26–28].

The dataset, consisting of 71 blend trials, was used to train the ML models to predict the CCI^*. To ensure robustness and reliability, 20 independent runs were performed, each employing 5-fold cross-validation, using different random seeds to split the data (between 11 and 32). Model performance was evaluated using the coefficient of determination (R^2), mean absolute error (MAE), and root mean squared error (RMSE). The average of these metrics across all seed runs was then computed to compare the accuracy and consistency of the models.

3 | Results and Discussion

3.1 | Rheological Characterization and Phase Inversion Calculation

The rheological properties of the neat polymers strongly influence the morphology of the obtained blend. Therefore, several models have been proposed for the calculation of the phase inversion point of two immiscible polymers empirically. This point is defined as the amount of secondary material needed to invert the morphology of a blend, in which the initial matrix material transforms into a dispersed phase and the initial dispersed phase converts into the matrix. Such models are summarized in Table 3. Although the Bourry-Favis or

TABLE 3 | Summary of some approaches to calculate the theoretical phase inversion of an immiscible two-component polymer blend system [5, 6, 29–31].

Model	Year	Equation[a]	Limitations
Jordhamo	1986	$\frac{\eta_1}{\eta_2} = \frac{\phi_1}{\phi_2}$	• Does not consider interfacial tension effect nor shear effect • Valid only for low viscosity contrasts
Utracki	1991	$\frac{\eta_1}{\eta_2} = \left(\frac{\phi_m - \phi_2}{\phi_m - \phi_1}\right)^{\eta_m \phi_m}$ $\eta_m = 0.84$ $\phi_m = 1.90$	• Assumption of simple shear flow • No interfacial tension • Valid only for low viscosity ratio < 4
Chen—Su	1993	$\frac{\phi_1}{\phi_2} = 1.2\left(\frac{\eta_1}{\eta_2}\right)^{0.3}$	• Requires experimental calibration of constants • Limited to Newtonian assumptions
Lyngaae-Jorgensen	1999	$\Phi_I = k\left(\phi - \phi_{cr}\right)^x$	• Requires morphological initial data • Based on percolation theory ⇒ limited to measurable transitions
Bourry-Favis	1998	$\phi_c = \frac{1}{1 + \left(\frac{\eta_1}{\eta_2}\right)^a (1 + \beta C a_c)}$	• Requires morphological initial data ⇒ droplet size and interfacial tension
Yu-Bausmina-Schreiber	2002	$\phi_c = \frac{1}{1 + \left(\frac{\eta_1}{\eta_2}\right)^{0.7} \left(1 + C\frac{\sigma}{\eta_2 \dot{\gamma}}\right)}$	• Requires morphological initial data ⇒ interfacial tension

[a]ϕ_i are volume fractions; ϕ_c is the critical volume fraction ratio between polymers at phase inversion; η_i are viscosities; σ is interfacial tension; $\dot{\gamma}$ is shear rate; β is an empirical constant between 0 to 5; Ca_c is the compatibilizer concentration; $C = 1$.

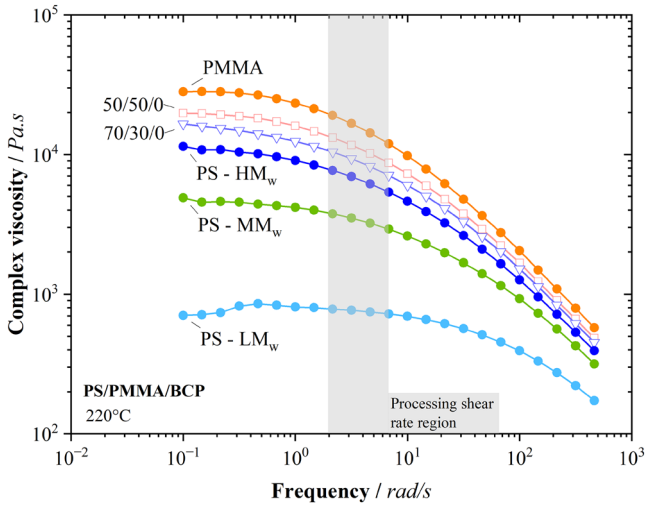

FIGURE 1 | Complex viscosity of neat polymers and selected blends with and without BCP addition in dependence of shear rate at 220°C.

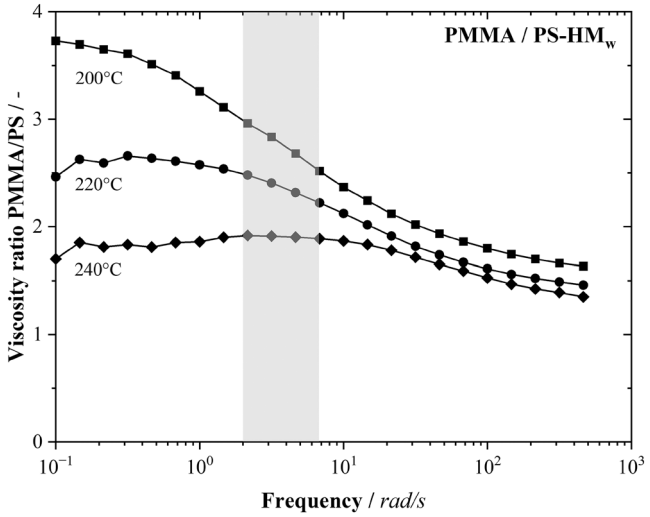

FIGURE 2 | Viscosity ratio between PMMA and PS-HM_W (high viscosity) in dependence of shear rate at different processing temperatures.

Yu-Bausmina-Schreiber models have been demonstrated to be more accurate by including the elasticity effect on their calculations, the materials in this research fulfill the assumptions of the simple models as well by having similar viscosities. In this study, we used Utracki's and Yu-Bausima-Schreiber equations to estimate the region in which phase inversion for the PS/PMMA blends occurs. The interfacial tension between materials used was 1.5 mN m^{-1} [32, 33]. The phase inversion point was determined using the viscosity ratios of the polymers at the processing parameters. Experimentally, it has been demonstrated that this is not a single point but a region (range of blend compositions) in which co-continuous phases are formed. Then, by gradually increasing the content of either of the polymers of the blend (PMMA or PS), the morphology will transform to a dispersed phase [4].

The complex viscosities of the neat polymers are shown in Figure 1 at 220°C in dependence of the shear rate. The gray shaded region indicates the shear rate applied during the manufacturing process between 22 and 52 s^{-1}, the last range was calculated using the rotational speed and the geometrical arrangement of the conical screws and the barrel. It is evident that the viscosity of PMMA is higher compared to all PS grades at the temperature and shear rates examined. For this research, we will focus on the smaller ratio between viscosities, selecting therefore the high viscosity PS (PS-HM_W). Also, it is possible to observe how the blends without BCP fall in between the neat materials curves. The effect of the diblock copolymer as well as the viscosity variation within the compositional range of the blend will be discussed in the following section.

The viscosity ratios between PMMA and PS-HM_W are shown in Figure 2, at the temperatures of processing. By increasing the temperature, the viscosities of the two components become more similar. The phase inversion can be calculated using Utracki and Yu-Bausmina-Schreiber models at the selected shear rates. The theoretical phase inversion composition ratios are summarized in Table 4. The results show that phase inversion for PS/PMMA blends can be obtained at compositions higher than 60–64 wt% of PMMA and 61–68 wt% PMMA, for the Utracki and Yu-Bausmina-Schreiber models, respectively. This indicates that in those regions morphology will start transforming to a PMMA matrix with dispersed PS. Below these PMMA contents, either a semi-co-continuous morphology may be possible (close to the lower PMMA content limit) or a matrix dominated by PS with dispersed PMMA phases will be obtained depending on the processing parameters. Interestingly, by applying both calculations to different processing conditions, the difference between the two models is just of 1 wt% at higher temperatures (where the viscosity ratio is smaller). At lower temperatures, the difference is increased to approximately 3–4 wt%. These results demonstrate the importance of considering interface behavior once the polymers viscosities are too different as it is done in the Yu-Bousima-Schreiber model [34, 35].

TABLE 4 | PMMA amount required for phase inversion calculated using Utracki and Yu-Bousmina-Schreiber models for shear rates of 60 and 150 rpm.

Temperature (°C)	Utracki		Yu-Bousmina-Schreiber	
	PMMA content (wt%)		PMMA content (wt%)	
	60 rpm	150 rpm	60 rpm	150 rpm
200	64.3	62.8	68.1	65.6
220	62.6	61.2	65.4	63.6
240	60.1	59.9	61.1	60.9

Regardless of the model, the predicted phase inversion point is affected mainly by temperature rather than the evaluated shear rate. This indicates that, in this system, the thermodynamics of mixing of the particular composition of the blend and the viscosity of its components will drive the morphology formation [36] rather than the shear stress applied during processing.

Experimentally, the morphologies observed by TEM are shown in Figure 3. This phase diagram corresponds to the blends without BCP addition manufactured under the same processing parameters (rotational speed: 60 rpm, temperature: 220°C, and residence time: 5 min) in which the PMMA (bright) and PS (dark) phases can be easily identified. The observed morphologies agreed with the prediction made by the rheological characterization and calculation, considering that the phase inversion experimentally occurs within a zone and not at a specific point [37]. There are two types of morphologies observed: a co-continuous for blends starting from a composition of 50/50 to 30/70 PS/PMMA and two dispersed phase zones in the form of droplets. Although completely co-continuous phases were not observed, an increase in the size and complexity of shape of dispersed phases below the inversion phase limit can be identified. This can be explained by the gradual formation of a co-continuous phase rather than an abrupt phase inversion [4].

3.2 | Effect of Diblock Copolymer on Polymeric Blends and the Co-Continuity Index

As expected, the addition of the PS-*b*-PMMA diblock copolymer, used as a compatibilizer, reduced the aspect ratio of the dispersed phases in the matrix-droplet morphologies (Figure S1). The droplet size reduction and stabilization can be attributed to a reduction of interfacial tension between PS and PMMA, thereby reducing

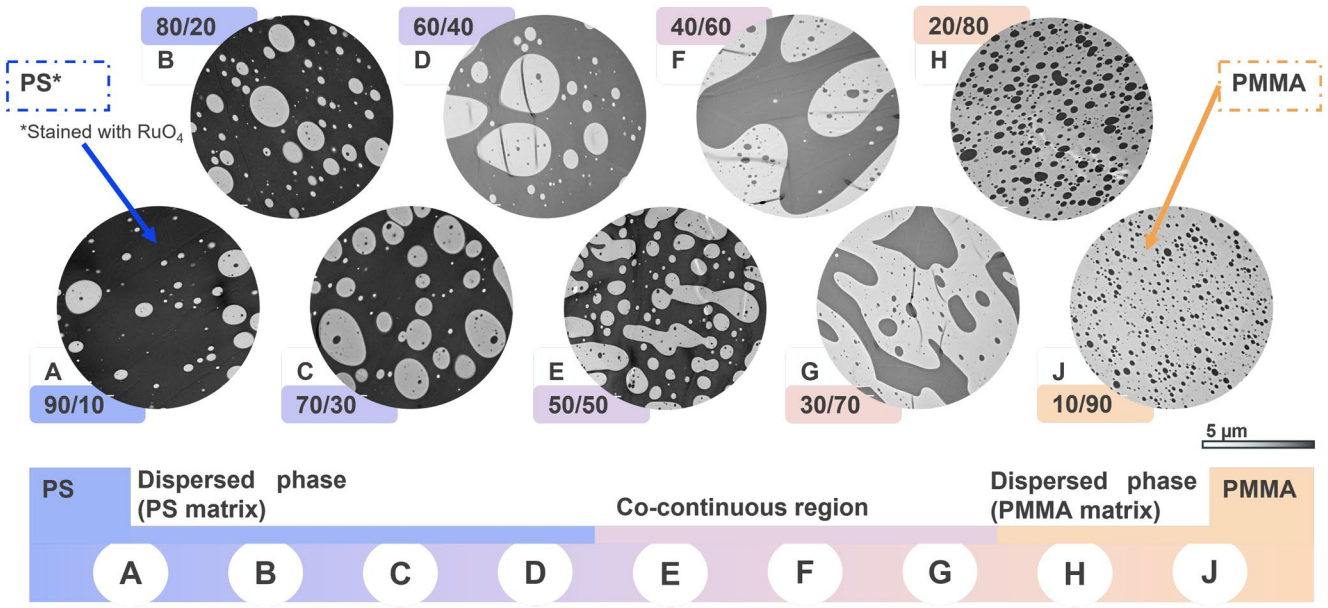

FIGURE 3 | Phase diagram of PS/PMMA blends without BCP compatibilizer manufactured at a residence time of 60 rpm, temperature of 220°C, and residence time of 5 min. Phase inversion point identification from dispersed phases.

coalescence in a dispersed morphology [7, 16, 38]. This behavior is thermodynamically consistent as the BCP is supposed to be located at the interfaces between immiscible polymer domains such as PS and PMMA [39, 40]. On the other hand, the selective location of the BCP inhibits the coarsening of the morphology in the region where the phase inversion was expected to occur. It also prevents break-up or merging of continuous domains. This ensures and facilitates the formation of finer co-continuous morphology. The theoretical models for phase inversion prediction used before cannot capture the complex interactions and properties of the compatibilizers with the polymers. Characteristics such as block length, block composition, or selective localization have an influence on morphology formation and are challenging to include in such models. To appropriately evaluate the effect of the BCP on the blends, rheological and thermo-mechanical properties were characterized for a set of blends with fixed processing parameters (Rotational speed: 60 rpm, temperature: 220°C, and residence time: 5 min).

The increase of phase interactions can be confirmed by the observed increase in complex viscosity (Figure 4) and the gradual decrease of the loss factor peak (Figure 5) with the addition of BCP. Both confirm that either a higher interaction between phases or better adhesion reduces the energy loss by slippage or friction [18, 39]. It was noticed that the glass transition temperature (T_g) of the PS was kept within similar values in each blend. While for the PMMA in the blends, the T_g was apparently affected by including the BCP gradually. The apparent increase in T_g of the PMMA can be attributed to the inclusion of syndiotactic PMMA, which is part of the BCP and has a higher T_g value than the PMMA homopolymer used in the blends [41]. The respective DSC traces and a comparison of T_g values can be found in the Figure S2. The storage modulus and loss modulus of the blends in Figure S3 do not show an evident variation with the addition of BCP at the evaluated temperature range; the effect is more clearly seen by the sensitivity of the loss factor.

The zero-shear viscosity was calculated from the respective flow curves for all blends studied. Figure 6 shows the evolution of zero-shear viscosity in dependence of the PMMA content in the blend and the amount of BCP added. First, without BCP, viscosity increases consistently toward the value of neat PMMA reaching a plateau approximately at 70 wt% addition. This is consistent with the transition from co-continuous to dispersed morphology with a PMMA matrix [34]. The initial decrease in viscosity is attributed to a lubrication effect due to the dispersed PMMA droplets in the PS matrix. On the other hand, at higher levels of PMMA (> 70 wt%), with a smaller dispersed phase size of PS (average area of 0.05 μm^2 in Figure 3H) than the dispersed PMMA (average area of 0.24 μm^2 in Figure 3B) observed, the interfacial interaction of the two components is increased creating higher resistance to flow [7]. By adding the BCP, the viscosity is increased for all compositions, being more pronounced for blends with higher PMMA contents. This increment also confirms that the location of the BCP is at the interface of the two blend phases, reducing not only the interfacial tension but enhancing the

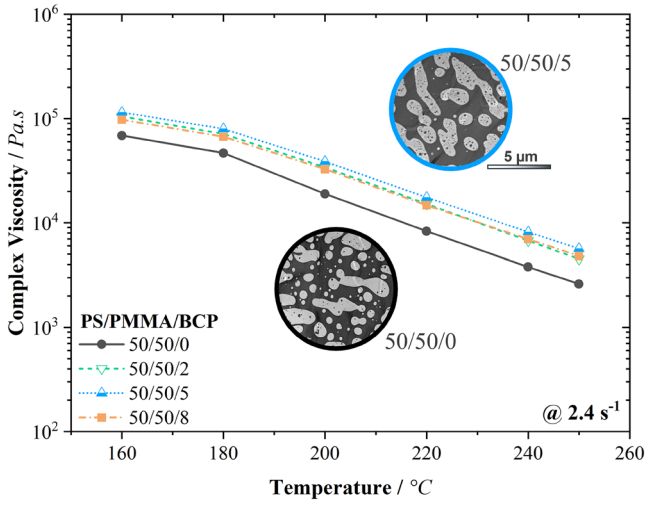

FIGURE 4 | Temperature dependence of complex viscosity of PS/PMMA 50/50 blends with different amount of BCP added during processing at a selected shear rate of 2.4 s^{-1}.

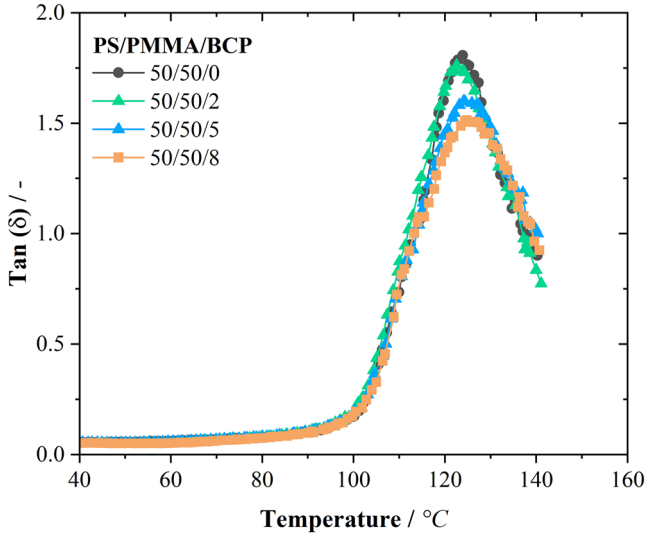

FIGURE 5 | Loss factor decrease effect due to the addition of BCP as compatibilizer in PS/PMMA 50/50 blends.

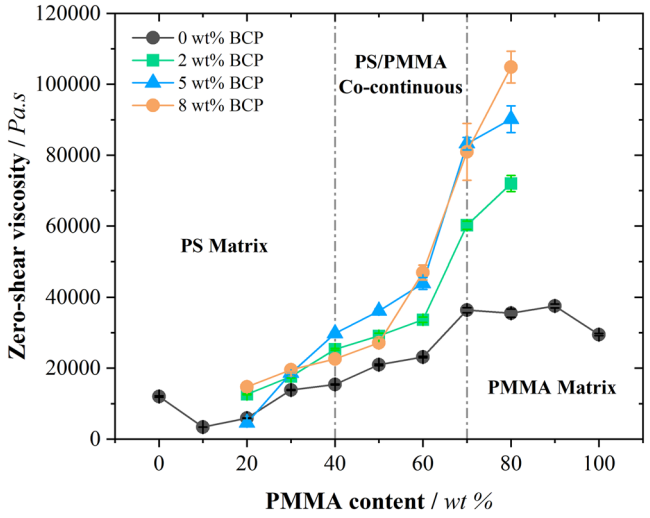

FIGURE 6 | Zero-shear viscosity determined as a function of PMMA content in the polymeric blends. Dotted limits were defined by the observation of the TEM images of each composition. The data were calculated at the reference processing temperature of 220°C.

interaction between the PS and PMMA domains [7, 39, 42]. Around the co-continuity zone identified by TEM on neat PS/PMMA blends Figure 3 (dotted vertical lines regions) the interfacial area increased. This promotes a higher interaction between the PS and PMMA facilitated by the BCP, generating a steep rise in elastic resistance and therefore in viscosity [34, 43]. The results are consistent with compatibilization theory, in which an appropriately designed BCP can fine-tune the interfacial structure, morphology formation, and viscoelastic behavior of immiscible polymer blends. Unfortunately, this rheological analysis will only provide a zone in which a co-continuous morphology may be located and not an optimal composition.

Therefore, a morphological examination was performed to identify the morphology with the highest degree of co-continuity. The effect of BCP addition on the blend morphology is shown in Figure 7 for the three most probable compositions for a co-continuous morphology as defined in the last section. Interestingly, at certain amounts of BCP (> 5 wt%) the three

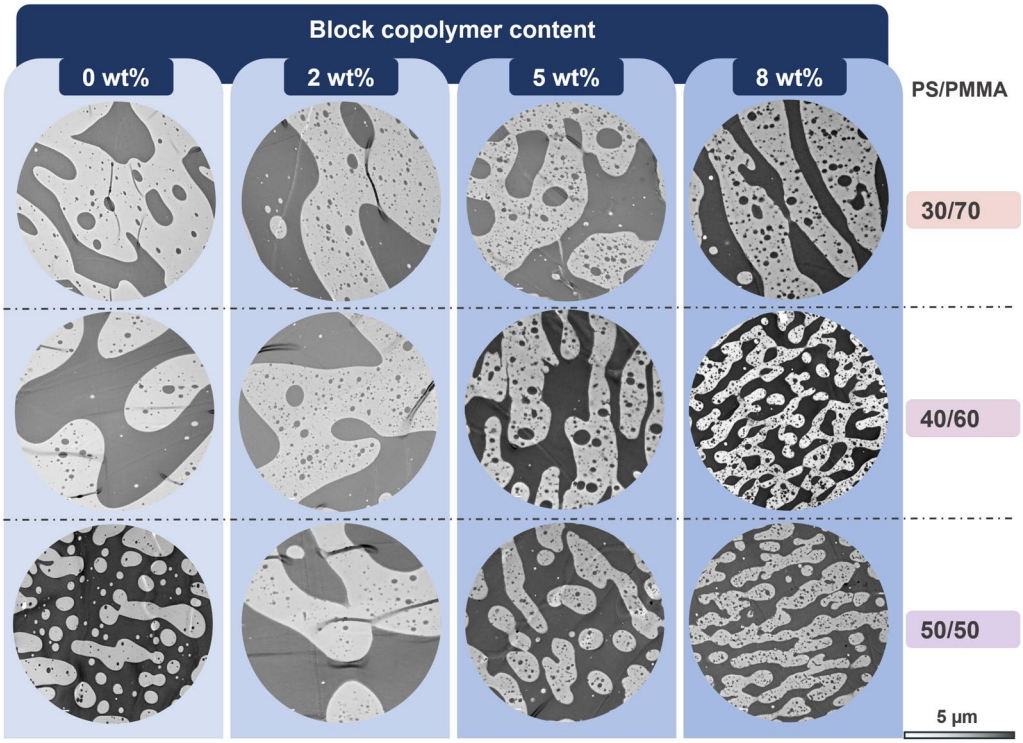

FIGURE 7 | Morphology modification in selected blends with different content of BCP compatibilizer. The variation of the *CCI** with BCP addition is available in the Supporting Information (Figure S4).

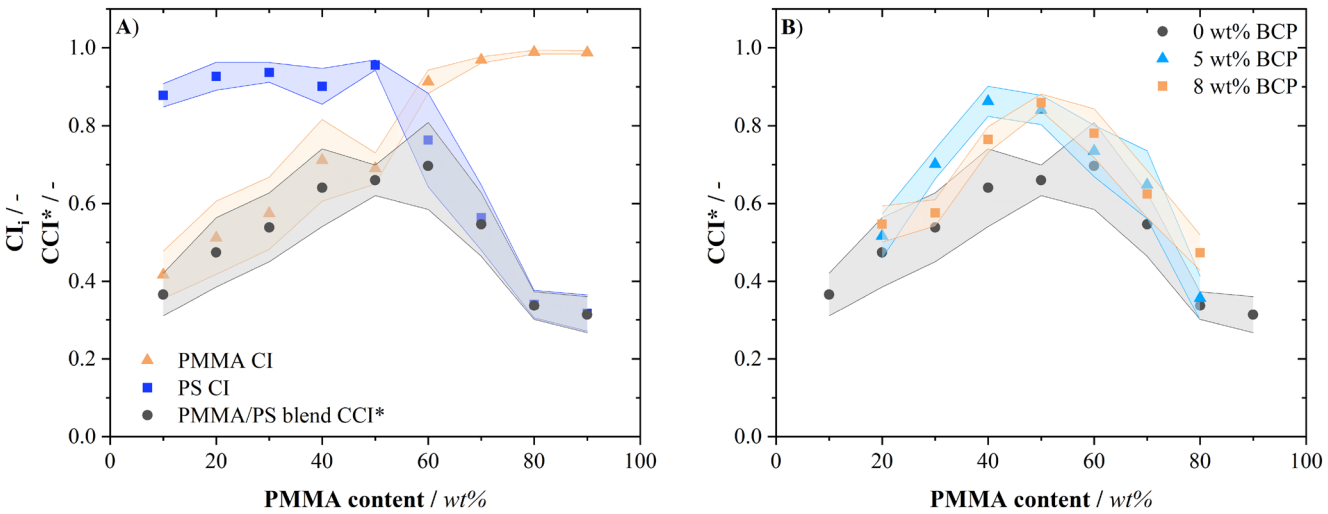

FIGURE 8 | (A) Continuity index (CI_i) calculation for each phase: PMMA (orange triangle), PS (blue square), and co-continuity index (CCI*) for blends without BCP addition (black circles). (B) Effect of adding BCP on the CCI* of the immiscible PS/PMMA blends. The average values are determined from several TEM micrographs at different positions and directions of the material. The shaded areas are the standard deviations of those calculations. Note that the maximum possible value for the continuous index and CCI* is 1.

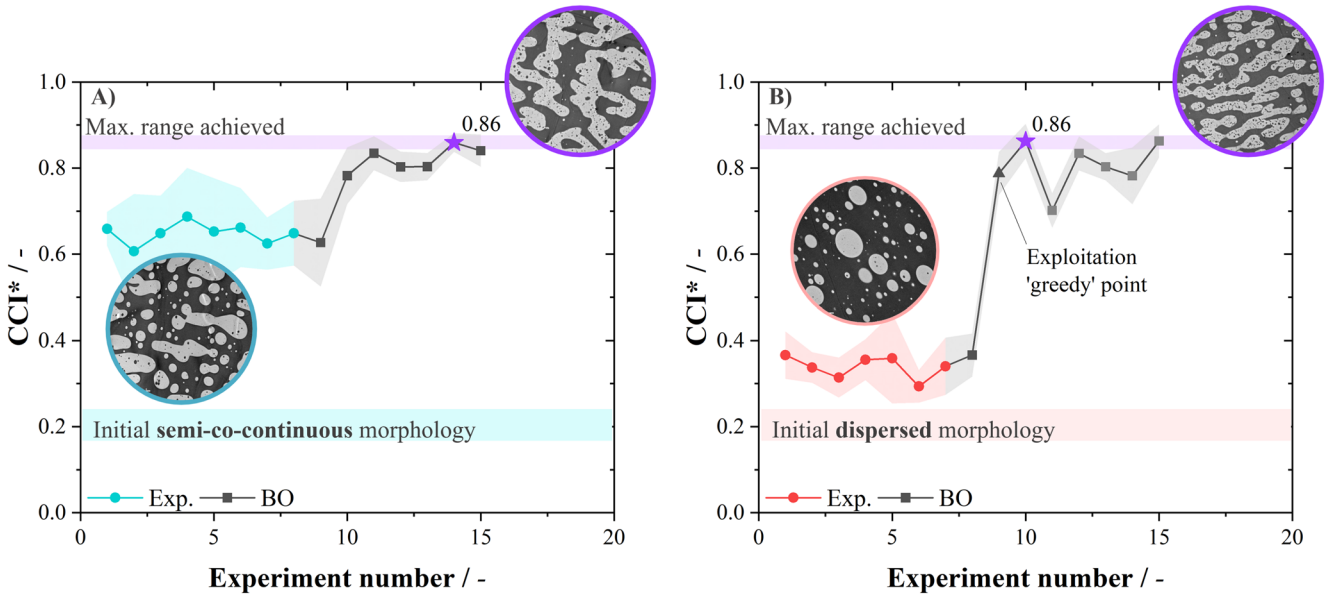

FIGURE 9 | (A) Bayesian optimization procedure applied to CCI* in PS/PMMA blends with semi-co-continuous morphology (blue) starting data and progression with every new BO point proposed (black). (B) Bayesian optimization applied to CCI* with a dispersed blend system (red) initial data and the progress of the BO proposals (black). The triangle corresponds to the 'greedy' suggestion. The points and shaded areas correspond to the average and standard deviation of the calculation of the CCI*. The purple star highlights the largest CCI* achieved. The parameters of each point could be seen in the Supporting Information Table S2.

compositions evaluated seem to have a co-continuous morphology with different phase sizes. To identify which of the observed morphologies have the highest degree of co-continuity, the co-continuity index (CCI*) was calculated using Equation (3) from the image analysis of the TEM results. The outcome can be seen in Figure 8 showing a clear difference between the dispersed zones and the co-continuous region. First, Figure 8A shows the progress of the continuity index (CI) of each individual phase on the blend. It is evident to observe the gradual increase in the continuity degree of each of the phases corresponding to the amount of polymer used in each blend. Second, it is also possible to observe the results of the CCI* calculation without the addition of BCP, in which the maximum co-continuity index is found for PMMA fractions between 40 and 60 wt% with CCI* values of 0.6 to 0.7, confirming the blend compositions found in previous research as co-continuous [7, 8, 21, 44]. In Figure 8B, it is possible to clarify the effect of BCP addition on the blends, increasing the gap difference in CCI* between a dispersed morphology and a co-continuous one. In this case, the maximum CCI* achieved is between 0.7 and 0.8 for the same compositional range evaluated before. This is explained by the ability of the BCP to compatibilize the interface and reduce the interfacial tension between the immiscible phases. At the critical point, where the co-continuous morphology occurs, the BCP containing blends more favorably stabilize in a co-continuous structure, enhancing networking of both phases and broadening the co-continuous regime [11, 15].

As demonstrated, the calculation of the CCI* parameter provides valuable information for the analysis of blend morphologies. Its relevance becomes particularly evident when phase inversion predictions are challenging, for instance due to the addition of complex interactions between additives or fillers, or when variations in blend properties are strongly driven by compositional factors rather than morphologies.

To achieve higher co-continuous blends, the definition of a clear and quantifiable descriptor -such as CCI*- is relevant for the implementation of machine learning-based optimization strategies. This approach supports a step-by-step design and manufacturing of blends with desired phase morphologies, while overcoming conventional theoretical and experimental challenges.

3.3 | Bayesian Optimization and Machine Learning Regression Modeling of Co-Continuity Index

For applying the Bayesian optimization using the experimental data, two cases were defined. The first case is close to the current blend system in which, on the basis of the information taken from the literature, an accurate approximation to a semi-co-continuous morphology with the initial set of experiments was done. The second case was considering a hypothetical scenario in which data of the blends are not available, so the initial data would contain only dispersed morphologies. In Figure 9 both cases are compared. For both, the maximum co-continuity index obtained is similar and the variability of the points is reduced, too. The number of experiments needed to achieve such a maximum varies depending on the situation. This is explained by the type of suggestion selected in every case. For the data that are closer to the co-continuous morphology, the experiments were selected using mainly the active learning and Bayesian standard approach due to the proximity to the ideal morphology. However, for the dispersed scenario, an exploitation 'greedy' point was selected, which drastically modified the optimization suggestions, leading to a faster finding of the maximum continuity. Combining both cases with the experimental data, it is possible to obtain an operational and compositional processing window to achieve a co-continuous morphology, as summarized in Table 5.

Additionally, with the experimental data collected, it is possible to apply the regression ML models proposed in this research to predict the CCI* of the blends. A simple linear regression model did not capture the relationship between the target (CCI*) and the factors of the experiment. Therefore, advanced models were explored. In Table 6, a summary of the evaluation metrics is shown for selected ML models. The selected metrics provide information on the precision and accuracy of the prediction [27]. None of the different models evaluated have a perfect fit of the prediction and the actual data, since the determination coefficient (R^2) is not close to 1. However, considering the evaluation of the models, the highest R^2 indicates better average performance, and the smallest MAE and RMSE shows greater precision. In this case, the random forest regressor was the best to fit the data evaluated, followed by the gradient boosting regressor with similar performance metrics. It is also important to note the small values of standard deviation obtained on each calculated parameter, which come from running several seeds with a 5-fold cross-validation, providing more robustness and precision to the results.

The relationship between the predicted (random forests) and actual values of CCI* in the blends can be seen in Figure 10A. It is evident that there are two different approximations of the points to the regression. On the one hand, in the zones of dispersed morphologies, CCI* < 0.6, the predictions show a significant large error compared to the co-continuous values. This fact is attributed to the limited amount of data obtained for dispersed morphologies, since the main objective of the research was to obtain the co-continuous phases, evidencing the importance of having a similar distribution of results for training the models. On the other hand, in the co-continuous zone, the data are diverse and distributed normally, which contributes to a better prediction and matching between predicted and observed values of CCI*.

TABLE 5 | Operational window parameters obtained through experimental and BO methods to obtain co-continuous morphologies in PS/PMMA/BCP blends.

Parameter	Units	Range
PMMA-content	(wt%)	46 ± 4
PS-content	(wt%)	54 ± 4
BCP-content (PMMA-*b*-PS)	(wt%)	6.2 ± 1.7
Temperature	(°C)	222.5 ± 2.5
Rotational speed	(rpm)	65 ± 5
Residence time	(min)	4 ± 1

Finally, a factor importance plot is shown in Figure 10B. According to the results, the most relevant factors that determine the morphologies in PS/PMMA blends are the weight fractions of PS, PMMA, and BCP. This aligns with the experimental observations, the theoretical and empirical approach, and the literature review. In such systems, the weight ratios of the two components and the compatibilizer (BCP), which will be located at the interphases, have a significant role over the processing parameters. Although processing parameters are secondary to

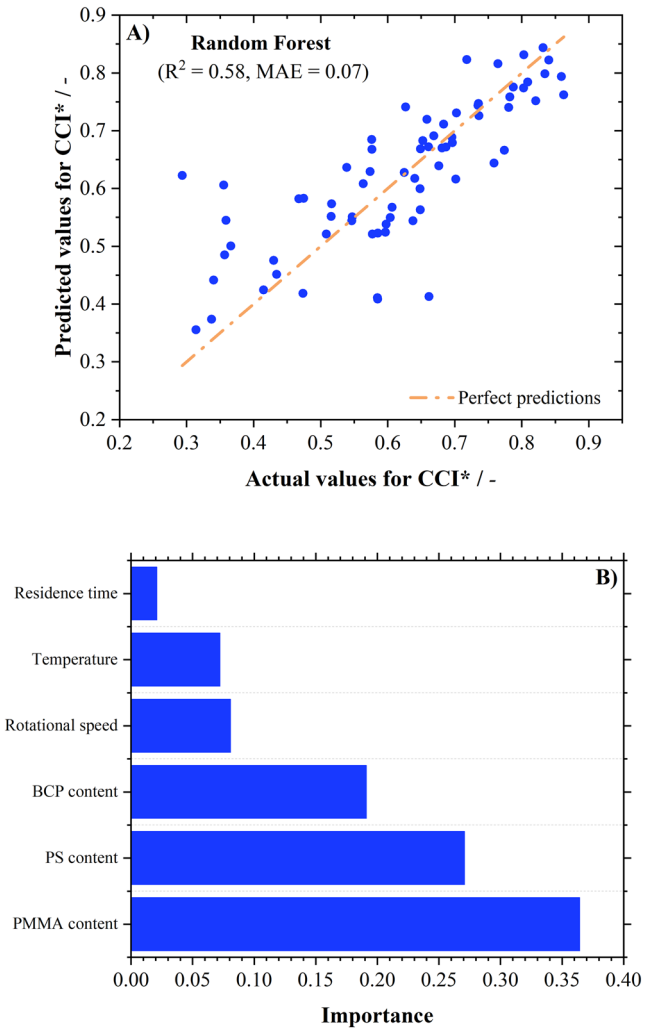

FIGURE 10 | (A) Comparison between the actual values and predicted values of the co-continuity index (CCI*) for the evaluated blends based on a random forest regression. (B) Composition and processing factors relevance based on the regression model applied.

TABLE 6 | Statistical metrics of the different models applied for predicting the co-continuity index for the evaluated polymer blends. Standard deviations refer to 20 repetitions of 5-fold cross validation runs.

Model	R^2	MAE	RMSE
Random forest	0.584 ± 0.078	0.065 ± 0.005	0.087 ± 0.006
Gradient boosting	0.518 ± 0.085	0.069 ± 0.005	0.093 ± 0.006
Support vector regressor	0.431 ± 0.061	0.088 ± 0.003	0.103 ± 0.004
Gaussian process (Const × Matern)	0.393 ± 0.110	0.078 ± 0.005	0.104 ± 0.006

the morphology formation, in this case, they must be selected properly to obtain the desired morphologies and to be able to properly process the materials [8, 9], especially temperature and shear rate (rotational speed).

4 | Conclusion

The phase inversion of immiscible PS/PMMA polymer blends was theoretically calculated using two different models. The inversion phase point was confirmed close to the experimental phase inversion region of the blends. The obtained morphologies were analyzed by TEM in which the matrix-dispersed phases were mainly seen at both < 40 wt% PMMA and > 70 wt% PMMA. The addition of BCP affects the blend morphology by stabilizing the morphology formation during processing, thus reducing the phase size, broadening the composition window of the co-continuous morphology, and improving the interfacial interaction between the interfaces, proved by DMA and viscosity measurements.

When polymer blends do not show significant differences in properties within different morphologies, this research demonstrates the importance of directly using the morphology observed via TEM to analyze and optimize the morphology formation itself, as demonstrated by calculating the co-continuity index.

Using Bayesian optimization (BO) combined with literature and experimental results, it is possible to determine processing and compositional windows for polymer blends in which certain morphologies or properties are desired. BO was able to maximize the co-continuity within only a few new experiments. This approach demonstrates potential to predict the formation of the co-continuous morphology under several processing and compositional factors using a random forest regressor. Robust modeling, with a larger dataset collected from the blends, could be obtained to improve the accuracy and precision of the model; especially in the dispersed morphology domains which were not further investigated in this research.

The results confirm that in the immiscible PS/PMMA blend system the morphology formation will be strongly influenced by the thermodynamical interactions between the two polymers rather than by the processing conditions, which agrees with the theoretical models evaluated at the selected temperatures and shear stresses. This methodology proves to be a relevant tool that could be extrapolated to polymer blending research and production to reduce time, resources, and experiments.

Author Contributions

Juan Felipe Castro-Landinez: conceptualization, methodology, investigation, writing – original draft, writing – review and editing, formal analysis, data curation, validation, visualization. **Tasmai Paul:** investigation, writing – original draft, writing – review and editing, validation, formal analysis, methodology, visualization. **Rodrigo Q. Albuquerque:** supervision, writing – review and editing. **Holger Schmalz:** supervision, writing – review and editing, formal analysis, validation. **Andreas Greiner:** conceptualization, project administration, resources, writing – review and editing, supervision. **Holger Ruckdäschel:** supervision, resources, project administration, conceptualization, writing – review and editing, writing – original draft.

Acknowledgments

We thankfully acknowledge the supply of polymeric material by INEOS Styrolution Group GmbH and Röhm GmbH. The support of the keylabs "Synthesis and Molecular Characterization" and "Electron and Optical Microscopy" of the Bavarian Polymer Institute (BPI) at Bayreuth University. The authors thank Rika Schneider for the GPC measurements. We also thank Annika Pfaffenberger and Ute Kuhn for the samples preparation and testing of TEM and DMA, respectively. This work has been supported by Collaborative Research Center 1585, project C04 of the German Research Foundation (grant number 492723217). Open Access funding enabled and organized by Projekt DEAL.

Funding

This work was supported by Deutsche Forschungsgemeinschaft (492723217).

Data Availability Statement

The data that support the findings of this study are available from the corresponding author upon reasonable request.

References

1. D. R. Paul and S. Newman, *Polymer Blends Volume 1* (Academic Press INC, 1978).

2. L. A. Utracki and C. A. Wilkie, *Polymer Blends Handbook* (Springer Netherlands, 2014).

3. A. I. Isayev, *Encyclopedia of Polymer Blends* (Wiley-VCH, 2010).

4. H. Ruckdäschel, J. K. W. Sandler, V. Altstädt, et al., "Compatibilisation of PPE/SAN Blends by Triblock Terpolymers: Correlation Between Block Terpolymer Composition, Morphology and Properties," *Polymer* 47, no. 8 (2006): 2772–2790.

5. J. W. Barlow and D. R. Paul, "Polymer Blends and Alloys—A Review of Selected Considerations," *Polymer Engineering & Science* 21, no. 15 (1981): 985–996.

6. J. W. Barlow and D. R. Paul, "The Importance of Enthalpic Interactions in Polymeric Systems," *Polymer Engineering & Science* 27, no. 20 (1987): 1482–1494.

7. C. W. Macosko, P. Guégan, A. K. Khandpur, A. Nakayama, P. Marechal, and T. Inoue, "Compatibilizers for Melt Blending: Premade Block Copolymers," *Macromolecules* 29, no. 17 (1996): 5590–5598.

8. J. K. Lee and C. D. Han, "Evolution of Polymer Blend Morphology During Compounding in an Internal Mixer," *Polymer* 40 (1999): 6277–6296.

9. J. K. Lee and C. D. Han, "Evolution of Polymer Blend Morphology During Compounding in a Twin-Screw Extruder," *Polymer* 41 (1999): 1799.

10. H. Ruckdäschel, J. K. W. Sandler, V. Altstädt, H. Schmalz, V. Abetz, and A. H. E. Müller, "Toughening of Immiscible PPE/SAN Blends by Triblock Terpolymers," *Polymer* 48, no. 9 (2007): 2700–2719.

11. M. Wu, H. Huang, and L. Yu, "Facile Approach for Largely Refining Phase Domains of PMMA/PS Blends and Improving Their Properties During Extrusion," *Polymer Testing* 93 (2021): 106918.

12. S. Thomas, R. Shanks, and S. Chandrasekharakurup, *Design and Applications of Nanostructured Polymer Blends and Nanocomposite Systems* (William Andrew Publishing, 2016).

13. S. Thomas, A. R. Ajitha, and M. Jaroszewski, *Polymer Blend Nanocomposites for Energy Storage Applications* (Elseiver, 2023).

14. D. R. Paul and S. Newman, *Polymer Blends Volume 2* (Academic Press INC, 1978).

15. G. Pu, Y. Luo, Q. Lou, and B. Li, "Co-Continuous Polymeric Nanostructures via Simple Melt Mixing of PS/PMMA," *Macromolecular Rapid Communications* 30, no. 2 (2009): 133–137.

16. B. Lin, U. Sundararaj, and P. Guegan, "Effect of Mixing Protocol on Compatibilized Polymer Blend Morphology," *Polymer Engineering & Science* 46, no. 5 (2006): 691–702.

17. S. Thomas and R. E. Prud'homme, "Compatibilizing Effect of Block Copolymers in Heterogeneous Polystyrene/Poly(Methyl Methacrylate) Blends," *Polymer* 33, no. 20 (1992): 4260–4268.

18. M. Yee, P. S. Calvão, and N. R. Demarquette, "Rheological Behavior of Poly(Methyl Methacrylate)/Polystyrene (PMMA/PS) Blends With the Addition of PMMA-*Ran*-PS," *Rheologica Acta* 46, no. 5 (2007): 653–664.

19. Y. Bussi, S. Golan, C. G. Dosoretz, and M. S. Eisen, "Synthesis, Characterization and Performance of PS/PMMA Blend Membranes for Potential Water Treatment," *Desalination* 431 (2018): 35.

20. T. Bubmann, A. Seidel, H. Ruckdäschel, and V. Altstädt, "Transparent PC/PMMA Blends With Enhanced Mechanical Properties via Reactive Compounding of Functionalized Polymers," *Polymers* 14, no. 1 (2021): 73.

21. M. Wu and H. Huang, "Enhancing Thermal Conductivity of PMMA/PS Blend via Forming Affluent and Continuous Conductive Pathways of Graphene Layers," *Composites Science and Technology* 206 (2021): 108668.

22. R. Q. Albuquerque, F. Rothenhäusler, and H. Ruckdäschel, "Designing Formulations of Bio-Based, Multicomponent Epoxy Resin Systems via Machine Learning," *MRS Bulletin* 49 (2024): 59–70.

23. R. Q. Albuquerque, F. Rothenhäusler, P. Groebel, and H. Ruckdäschel, "Multi-Objective Optimization of Sustainable Epoxy Resin Systems Through Bayesian Optimization and Machine Learning," *ACS Applied Engineering Materials* 1 (2023): 3298–3308.

24. K. A. Shah, R. Q. Albuquerque, C. Brütting, M. Dippold, and H. Ruckdäschel, "Low-Density Polyamide 12 Foams Using Bayesian Optimization and Inverse Design," *Polymer* 320 (2025): 128096.

25. S. Takasuka, S. Ito, S. Oikawa, et al., "Bayesian Optimization of Radical Polymerization Reactions in a Flow Synthesis System," *Science and Technology of Advanced Materials, Methods* 4, no. 1 (2024): 2425178.

26. S. M. Pai, K. A. Shah, S. Sunder, R. Q. Albuquerque, C. Brütting, and H. Ruckdäschel, "Machine Learning Applied to the Design and Optimization of Polymeric Materials: A Review," *Next Materials* 7 (2025): 100449.

27. K. A. Shah, C. Brütting, R. Q. Albuquerque, and H. Ruckdäschel, "Machine Learning Investigation of Polylactic Acid Bead Foam Extrusion," *Journal of Applied Polymer Science* 141, no. 30 (2024): e55693.

28. R. Q. Albuquerque, C. Brütting, T. Standau, and H. Ruckdäschel, "A Machine Learning Investigation of Low-Density Polylactide Batch Foams," *E-Polymers* 22, no. 1 (2022): 318–331.

29. G. M. Jordhamo, J. A. Manson, and L. H. Sperling, "Phase Continuity and Inversion in Polymer Blends and Simultaneous Interpenetrating Networks," *Polymer Engineering & Science* 26, no. 8 (1986): 517–524.

30. T. H. Chen and A. C. Su, "Morphology of Poly(*p*-Phenylene Sulfide)/Polyethylene Blends," *Polymer* 34, no. 23 (1993): 4826–4831.

31. L. A. Utracki, "On the Viscosity–Concentration Dependence of Immiscible Polymer Blends," *Journal of Rheology* 35, no. 8 (1991): 1615–1637.

32. H. Gramespacher and J. Meissner, "Melt Elongation and Recovery of Polymer Blends, Morphology, and Influence of Interfacial Tension," *Journal of Rheology* 41 (1997): 27–44.

33. K. Okamoto, M. Takahashi, H. Yamane, H. Watashiba, Y. Tsukahara, and T. Masuda, "Measurement of Interfacial Tension Between Polymer Melts: Improved Imbedded Fiber Retraction, Breaking Thread and Dynamic Viscoelasticity Methods," *Nihon Reoroji Gakkaishi* 27, no. 2 (1999): 109–115.

34. F. A. Versteeg, A. Mukherjee, F. Picchioni, and D. Parisi, "Phase Inversion Detection in Immiscible Binary Polymer Blends via Zero–Shear Viscosity Measurements," *Polymer Engineering & Science* 64, no. 7 (2024): 3160–3172.

35. K. El Mabrouk and M. Bousmina, "Assessment of Morphology in Transient and Steady State Regimes Resulting From Phase Separation in Polystyrene/Poly(Vinyl Methyl Ether) Blend," *Rheologica Acta* 45, no. 6 (2006): 877–889.

36. E. Manias and L. A. Utracki, "Thermodynamics of Polymer Blends," in *Polymer Blends Handbook*, ed. L. Utracki and C. Wilkie (Springer, 2014).

37. L. A. Utracki, *Polymer Blends Handbook* (Kluwer Academic Publishers, 2002).

38. J. Liu, H. Guo, X. Pang, et al., "Dynamics of Polystyrene-*Block*-Poly(Methyl Methacrylate) (PS-*b*-PMMA) Diblock Copolymers and PS/PMMA Blends: A Dielectric Study," *Journal of Non-Crystalline Solids* 359 (2013): 27–32.

39. I. Fortelný and J. Jůza, "The Effects of Copolymer Compatibilizers on the Phase Structure Evolution in Polymer Blends-A Review," *Materials* 14, no. 24 (2021): 7786.

40. Y. Xu, C. M. Thurber, C. W. Macosko, T. P. Lodge, and M. A. Hillmyer, "Poly(Methyl Methacrylate)-*Block*-Polyethylene-*Block*-Poly(Methyl Methacrylate) Triblock Copolymers as Compatibilizers for Polyethylene/Poly(Methyl Methacrylate) Blends," *Industrial & Engineering Chemistry Research* 53, no. 12 (2014): 4718–4725.

41. K. Chat, W. Tu, A. Beena Unni, and K. Adrjanowicz, "Influence of Tacticity on the Glass-Transition Dynamics of Poly(Methyl Methacrylate) (PMMA) Under Elevated Pressure and Geometrical Nanoconfinement," *Macromolecules* 54, no. 18 (2021): 8526–8537.

42. F. S. Bates and G. H. Fredrickson, "Block Copolymers—Designer Soft Materials," *Physics Today* 52, no. 2 (1999): 32–38.

43. C. D. Han, "Compatibilization of Two Immiscible Homopolymers," in *Rheology and Processing of Polymeric Materials: Volume 2: Polymer Processing* (Oxford University Press, Inc., 2007).

44. J. Wie and J. Kim, "Thermal Conductivity Enhancement Derived From Poly(Methyl Methacrylate)-Grafted Carbon Nanotubes in Poly(Methyl Methacrylate)/polystyrene Blends," *Polymers* 11, no. 8 (2019): 1347.

Supporting Information

Additional supporting information can be found online in the Supporting Information section. **Figure S1:** Morphology modification in a dispersed morphology blend (PS/PMMA 70/30) with different content of BCP. **Figure S2:** (A) DSC curves and glass transition temperature for the neat materials PS, PMMA, and the two batches of BCP used as compatibilizer. (B) Glass transition temperature variation for each material in the prepared blends as a function of the BCP content. **Figure S3:** (A) Storage modulus and (B) Loss modulus variation of the polymer blends as a function of the added block copolymer evaluated at different temperatures in tension mode. **Figure S4:** Co-continuity index of the selected polymer blends variation with varying concentration of diblock copolymer. **Figure S5:** Molecular weight distribution measured by GPC in THF for the PS precursor and the diblock copolymer PS-b PMMA. **Figure S6:** TEM micrograph of a solution cast film of the PS-b-PMMA diblock copolymer in THF, showing a lamellar morphology. The microtome sliced film was stained with RuO4, for the PS phase to appear dark. **Table S1:** Blends composition set for the initial experimental trials. **Figure S7:** 1H-NMR spectra of PS-b-PMMA measured in CDCl3 ($\delta = 7.26$ ppm) at 300 MHz and 64 scans. For both BCP batches produced (A) First BCP batch BCP01 and (B) Second BCP batch synthesized BCP02. **Table S2:** Experimental (Exp.) parameters used only for the Bayesian Optimization procedure and the corresponding experiments suggestion sthrough (BO).